

Lipid organization in pig stratum corneum

J. A. Bouwstra,^{1,*} G. S. Gooris,^{*} W. Bras,[†] and D. T. Downing^{**}

Leiden/Amsterdam Center for Drug Research,^{*} P.O. Box 9502, 2300 RA, Leiden, The Netherlands; Netherlands Organization for Scientific Research/SERC Daresbury,[†] Warrington, WA4AD, United Kingdom; and Marshall Dermatology Research Laboratories,^{**} University of Iowa, Iowa City, IA

Abstract The lipid and keratin structure of pig stratum corneum has been elucidated by small- and wide-angle X-ray diffraction. The measurements were carried out as a function of hydration and temperature. In addition, the stratum corneum was measured after recrystallization of the lipids at various temperatures. The results led us to conclude that the intercellular lipids in the stratum corneum are organized in at least two different lamellar structures with repeat distances of 6 and 13.2 nm. There is an indication for the presence of a third phase with a periodicity of 9 nm. The wide-angle pattern revealed a hexagonal (0.414 nm spacing) and liquid lateral packing (≈ 0.46 nm spacing). The 0.414 nm reflection started to decrease in intensity between 60 and 66°C and disappeared between 72 and 95°C. Furthermore, crystalline cholesterol has been indicated by both, wide- and small-angle X-ray diffraction, while the reflections of α -keratin were observed in the wide-angle X-ray diffraction pattern.—**Bouwstra, J. A., G. S. Gooris, W. Bras, and D. T. Downing.** Lipid organization in pig stratum corneum. *J. Lipid Res.* 1995. 36: 685–695.

Supplementary key words lipids • keratin • X-ray diffraction

A major function of the outermost layer of the skin, the stratum corneum (SC), is to provide a barrier to evaporation of water from underlying viable cell layers and to protect the organism against undesirable substances from the environment. The SC consists of dead flattened cells, the corneocytes, embedded in lipid lamellar regions. The interior of the corneocytes is filled with keratin. It has been found that drugs are mainly transported through the intercellular lamellar regions (1) and that consequently the barrier function of the skin relies mainly on these lamellar phases. Therefore, knowledge of the phase behavior of the lipids is of great importance in understanding the barrier function of the skin. The major lipids present in the SC are ceramides, cholesterol, and free fatty acids (2, 3). Stratum corneum ceramides represent a unique heterogeneous group of structures. No phospholipids are found in the outermost layer of the skin. In recent years the lipid structure of the stratum corneum has been studied using small- and wide-angle X-ray diffraction (4–8) and electron microscopy (9–11). Using small (SAXD) and wide (WAXD) angle X-ray diffraction, several aspects of the

structures of human and mouse SC have been elucidated. In human SC, two lamellar structures were found with repeat distances of approximately 6.4 and 13.4 nm, respectively. In mouse SC, a 13.2 nm periodicity was observed (4) while, occasionally, a 6 nm lamellar phase also could be found (8).

The lipid chain packing in human and mouse SC is orthorhombic. This was based on the 0.375 and 0.415 nm reflections present in the WAXD pattern. Possibly a hexagonal chain packing is present also, but the corresponding reflection at 0.415 nm was obscured by the 0.415 nm reflection of the orthorhombic structure. In mouse SC, a liquid-like chain packing was also found. The presence of a liquid-like packing could not be determined in human stratum corneum, because the corresponding 0.46 nm diffuse ring is obscured by the diffraction pattern of amorphous keratin. Differences in chain packing might partly explain differences in diffusional resistance in the SC.

In this study the lipid structure of pig SC has been elucidated using SAXD and WAXD. Pig SC is of interest as this tissue has been widely used as a model for human SC. Electron microscopy with RuO₄ post-fixation revealed that the intercellular lipids in pig SC are arranged in lamellae and that these lamellae form the characteristic Landmann units (12), which consist of a pattern of two broad and one narrow electron-lucent bands, between which electron-dense bands are located. This pattern has also been observed in human (11) and mouse SC (9). So far no studies have been reported on the lipid structure of intact pig SC or isolated corneocyte envelopes using X-ray diffraction. Very recently, one study was carried out on the physical structure of lipids extracted from pig stratum corneum (13). It appeared that the acetone-extracted lipids form a long periodicity structure of approximately 13.5 nm, while chloroform-methanol-extracted lipids form a single layered phase with a periodicity of 5.4 nm.

Abbreviations: SC, stratum corneum; SAXD, small-angle X-ray diffraction; WAXD, wide-angle X-ray diffraction; PBS, phosphate-buffered saline.

¹To whom correspondence should be addressed.

EXPERIMENTAL

Stratum corneum samples

The SC was separated from the epidermis by digestion with 0.1% trypsin in phosphate-buffered saline (PBS, pH 7.4) at 37°C. The stratum corneum was subsequently treated with a 0.1% inhibitor (Type II-S from Soybean, Sigma Chemicals, The Netherlands). After rinsing in water, the SC was dried over silica gel. Before use, the SC was hydrated over 27% (w/w) NaBr solution (resulting in an approximate 20% hydration of SC), water (hydration level of SC 60%), or silica gel (hydration level of SC 6%). The hydration level of SC has been defined as $100\% \times (\text{weight hydrated SC} - \text{weight dry SC}) / \text{weight hydrated SC}$.

Corneocyte envelope

Corneocytes were isolated from pig epidermis essentially as described previously (14). After shaving the dead animal, sheets of epidermis were removed by brief heat treatment (65°C, 30 sec) followed by scraping. The epidermal pieces were treated with 0.2% trypsin overnight to allow isolation of the stratum corneum. The stratum corneum was then digested overnight in 8 mM N,N-dimethyldodecylamine oxide/2 mM sodium decylsulfate at 45°C, which disintegrated the tissue into corneocyte envelopes. Sonication was not used, allowing the recovery of intact envelopes. Hair and any undigested material were then removed by passing the digest through a fine polyester mesh. The filtrate was centrifuged and the supernatant, containing lipids and solubilized keratin, was discarded. The pellet was treated repeatedly by overnight heating in the detergent mixture until the discarded supernatant was no longer cloudy. The pellet was then washed several times with distilled water and the final pellet was lyophilized. Electron microscopy after RuO₄ fixation showed that the resulting preparation consisted almost exclusively of empty intact corneocyte envelopes.

Small-angle X-ray scattering

All measurements were carried out at the Synchrotron Radiation Source at Daresbury Laboratory (Warrington, UK) using station 8.2. This station has been built as part of a NWO/SERC agreement. The camera produces a slightly converging beam with a very high intensity and a wavelength of 0.152 nm. The small-angle camera was equipped with a position-sensitive quadrant detector. The sample-to-detector distance was set to 1.80 m. The scattered intensities were corrected for primary-beam decay and absorption of X-rays by the sample, using two ion chambers which are placed on either side of the sample. This enables direct comparison between the intensities of the various scattering curves. The camera is able to produce a focal spot with a beam cross section of $0.3 \times$

4 mm². A more detailed description of the experimental set up has been given elsewhere (6).

A stack of stratum corneum sheets was loaded in the temperature-controlled sample cell. The temperature of this sample cell can be adjusted between 25 and 200°C. Care was taken that the incoming beam was parallel to the stratum corneum plane. Data collection was carried out for a period of 15 min for each sample. Checks for the appearance of radiation damage were performed but proved to be negative (6). The scattering intensity of the empty cell was measured and after normalization subtracted from the curves of the cell filled with sample. The scattering intensities have been plotted as a function of the scattering vector Q , defined as $Q = (4 \pi \sin \theta) / \lambda$, in which λ and θ are the wavelength and scattering angle, respectively. The positions of the diffraction peaks are directly related to the periodicity of the molecular structure as described by Bragg's law $2 d \sin \theta = n \lambda$, in which n and d are the order of the diffraction peak and the repeat distance, respectively. In the case of a lamellar structure, the various peaks are located at equidistant positions, which are given by the equation $Q_n = 2 n \pi / d$, in which Q_n is the position of the n th order reflection.

Diffraction curves of SC were measured under the following conditions: 1) porcine SC hydrated to various water contents; 2) 20% w/w hydrated SC at elevated temperatures; 3) 20% w/w hydrated SC heated to 55°C, 66°C, 79°C, or 109°C and subsequently cooled to ambient temperature in order to recrystallize the lipids; and 4) isolated corneocyte envelopes as function of temperature at 20% w/w hydration.

Wide-angle X-ray scattering

The diffraction patterns were obtained with the fiber diffraction camera at station 7.2 of the Synchrotron Radiation Source in Daresbury. A more detailed description of the camera is given elsewhere (7). The temperature-controlled sample holder was placed inside a He-filled chamber in order to reduce air scatter and absorption. The stratum corneum samples were stacked. The incoming beam was parallel to the stratum corneum surface, with the exception of one measurement in which the stratum corneum plane was located perpendicular to the primary beam. To avoid evaporation of water, the sample cell was sealed with mica windows. Patterns were recorded on CEA X-Ray films. Three films were mounted simultaneously in the film holder in order to increase the dynamic range of the film material. The sample to film distance was set to 9.3 cm. The scattering angle (θ) varied between 1.4° and 15°, corresponding to spacings varying in a range between 0.3 and 3 nm. In this paper, the position of the reflections will be denoted by their spacings. The primary beam path length through the sample was 1 mm. The temperature of the sample cell could be ad-

justed between 25°C and 120°C using a heating wire in combination with a thermocouple located in the sample cell.

The diffraction patterns of SC were measured under the following conditions: 1) SC hydrated to various levels; 2) SC at 45°C, 55°C, 66°C, 79°C, or 109°C; 3) SC heated to 55°C or 120°C and cooled to ambient temperature in order to recrystallize lipids; 4) chloroform-methanol-extracted SC; and 5) isolated corneocyte envelopes as a function of temperature.

RESULTS

If not stated otherwise, the results below were obtained with SC sheets orientated parallel to the primary beam.

Lamellar phases

Room temperature measurements. Several features could be distinguished on the SAXD curve of pig SC at 20% w/w hydration. The curve is plotted in Fig. 1. The main position of the strongest peak, located at $Q = 1.05 \text{ nm}^{-1}$, corresponds to a spacing of 6.0 nm. There is a shoulder on the main peak at $Q = 1.4 \text{ nm}^{-1}$ (spacing 4.5 nm). Furthermore, at low Q on the descending scattering curve, two shoulders are located (see arrows). Due to the steep baseline, the positions and spacings of these reflections could not be determined with high accuracy, but are approximately 9 and 12 nm, respectively. At higher Q values (see inset in Fig. 1) one sharp peak at $Q = 1.88 \text{ nm}^{-1}$ (spacing 3.35 nm) and several weak reflections at approximately 2.09 nm^{-1} (spacing 3.0 nm), 2.3 nm^{-1} (spacing 2.7 nm), and 2.86 nm^{-1} (spacing 2.2 nm) are observed. The positions of these weak reflections were difficult to determine due to their low intensities, but the 3.0, 2.7, and 2.2 nm diffraction peaks were confirmed by wide angle X-ray measurements (see below).

The WAXD pattern, which is shown in Fig. 2, revealed diffraction arcs, located close to the primary beam, that are higher order reflections of the same lipid phases as detected by SAXD. The spacings of these reflections (3.35, 3.0, 2.67, 2.2, 1.68, 1.54, and 1.32 nm) indicate that these are higher order reflections from the same lamellar phases as detected by SAXD. The strongest intensities of the arcs were located on the meridian, indicating that the lamellae were mainly aligned parallel to the surface of the SC.

Pig stratum corneum as a function of hydration. The diffraction curves as a function of the water content are depicted in Fig. 1. Increase in hydration level did not change the various peak positions, except for a very small increase in spacing when comparing the 60% curve and the curve indicated by dry (6% hydration). Increase in hydration level from 6 to 60% resulted in an increase of only 0.1 to 0.2 nm in spacing. This justifies the conclusion that almost no swelling of the lamellae occurred upon hydration of the SC. This was also observed in human and mouse SC (6,

9). This indicates that most of the water is located in either corneocytes or in a separate phase in the intercellular regions. In a recent study (15), a PBS solution was applied on human stratum corneum for 48 h, after which the stratum corneum was visualized by freeze fracture electron microscopy. The electron micrographs revealed the presence of swollen corneocytes and the presence of water pools in the intercellular regions. The latter denotes that at high water uptake phase separation takes place between lipids and water. Furthermore, the shoulder of the main peak of the diffraction curve (4.5 nm spacing) increased in intensity upon hydration; this behavior was also often encountered in SC samples obtained from other pigs.

Pig stratum corneum at elevated temperatures. The scattering curves of samples hydrated to 20% (w/w) measured at elevated temperatures are shown in Fig. 3 and Table 1. Although the X-ray scattering data were corrected for beam decay of the synchrotron source and for X-ray absorption of the sample, which makes the intensities of the curves directly comparable, it is rather difficult to quantify the intensities of the 6 and 4.5 nm peaks as function of temperature. a) The two peaks are not resolved (mainly due to the limited number of lamellae between the cells);

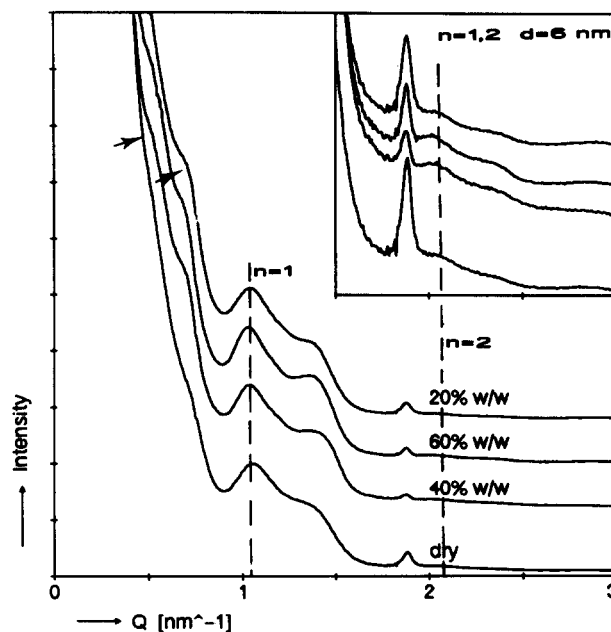


Fig. 1. The diffraction curve of pig SC at various hydration levels as indicated in the figure. Various diffraction peaks and shoulders are depicted. The two arrows at the steep descending curves indicate two shoulders corresponding to spacings of 12 and 9 nm, respectively. The main position of a strong diffraction peak is a first order diffraction peak of a 6 nm lamellar phase. The intensities are in arbitrary units. In the inset the curves are plotted in the same sequence at another intensity scale, but at the same Q -scale. In the inset Q ranges from 1.5 nm^{-1} to 3.0 nm^{-1} . The vertical dotted lines refer to the first and second order diffraction peak of the 6 nm lamellar phase.

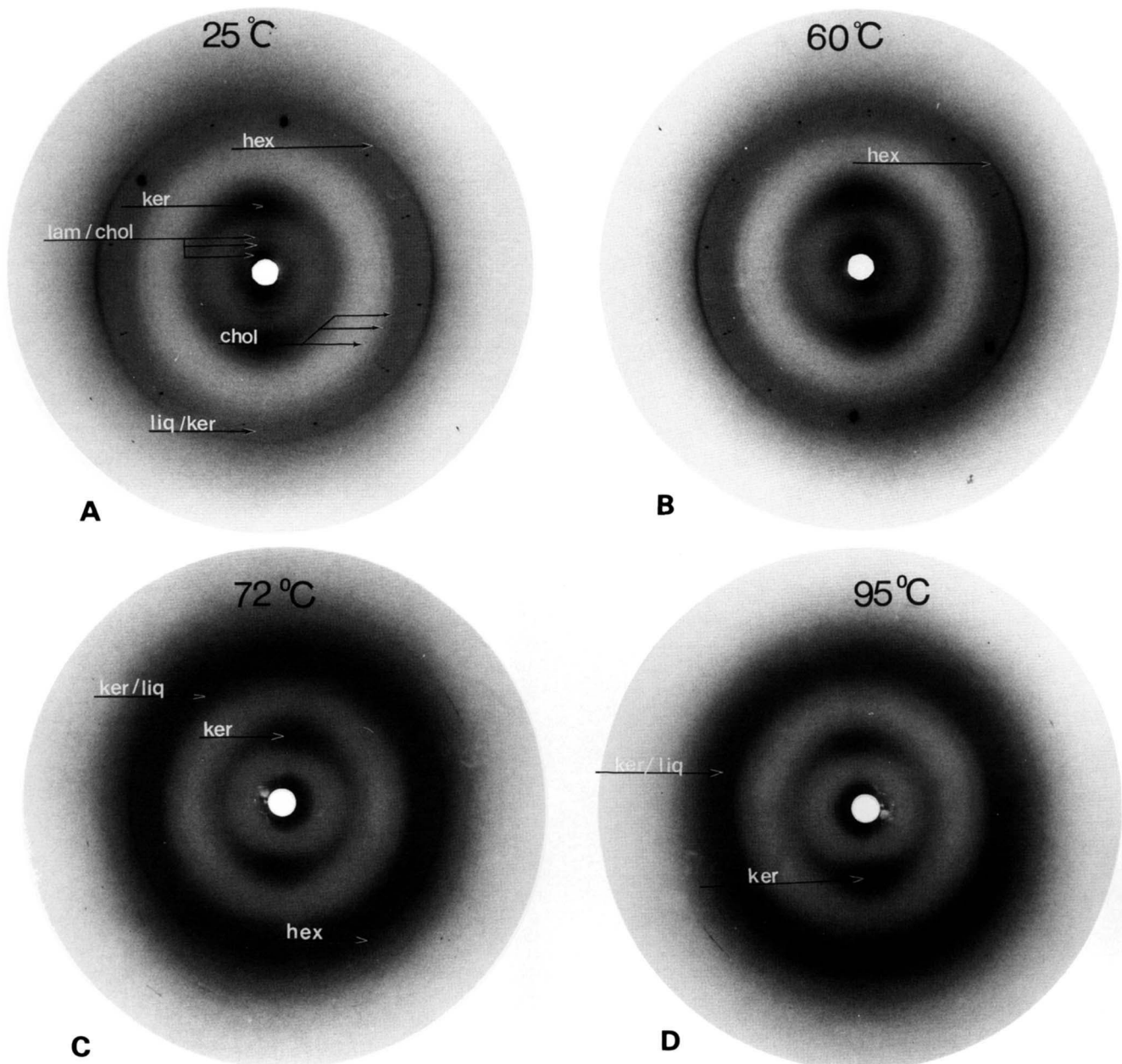


Fig. 2. A: The WAXD diffraction pattern of pig stratum corneum at 25°C. The cholesterol, keratin, lateral packing, and lamellar reflections are all indicated in the figure. The high intensity dots are caused by the mica windows. B: The WAXD diffraction pattern of pig stratum corneum at 60°C. The cholesterol, keratin, and lateral reflections are indicated in Fig. 2A. A sharpening of the 0.414 nm reflection is observed compared to that at 25°C. C: The WAXD pattern of pig SC at 72°C. Only a weak 0.414 nm reflection was detected. The cholesterol reflections and the reflections based on the lamellae disappeared between 60 and 72°C. D: The WAXD pattern of SC at 95°C.

b) both peaks vary in intensity as a function of temperature; and *c)* a possible presence of the broad peak observed at 66°C at lower temperatures as well. Although no quantification could be made, it was possible to observe trends in peak intensity changes as a function of temperature. The temperature was varied between 22 and 66°C. Upon heating the sample, there was almost no shift in the 6 nm peak position observed. The corresponding spacings and approximate intensities are given in Table 1. Between

22°C and 50°C an increase in the intensity of the 4.5 nm shoulder was found. This behavior was consistent in SC obtained from different pigs. Between 50 and 55°C, the 9 nm shoulder ($n = 1$ in Fig. 3) disappeared. Furthermore, between 50 and 55°C the 4.5 nm shoulder ($n = II$) weakened strongly and possibly disappeared also, while the 6 nm peak ($n = 1$ in Fig. 3) decreased in intensity but was still clearly present. Indications were found that the 9 and 4.5 nm peaks are partly based on the same lamellar

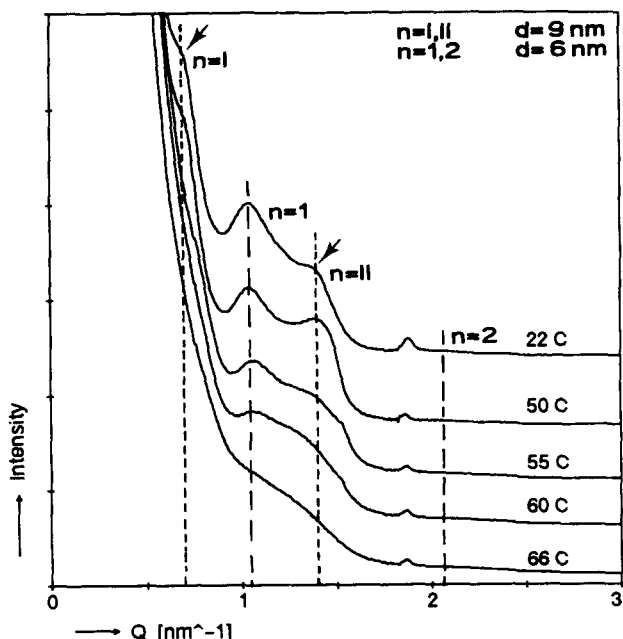


Fig. 3. The SAXD curves at various temperatures as indicated in the figures. The 9 and 4.5 nm shoulders on the curve both seemed to disappear at 55°C (see arrows), which indicated that the reflections are based on the same phase. The intensities are in arbitrary units.

phase, which confirms the weakening of the 4.5 nm peak between 50 and 55°C. Furthermore, from these observations and from recrystallization experiments (see below), it was concluded that the 4.5 nm shoulder and the 6 nm

peak originate from different lipid phases. Between 55°C and 60°C the intensity of the 6.0 nm peak ($n = 1$) weakened but seems still to be present at 60°C. At 66°C only a very broad shoulder, and the 3.35 nm peak, were detected on the diffraction curve.

Scattering curves after recrystallization of the lipids from various temperatures. The SC was heated to various temperatures, allowed to equilibrate for 1 h, and subsequently cooled to ambient temperatures. The resulting scattering curves are shown in **Fig. 4A and B** and the corresponding spacing in **Table 2**. The curves drawn in the inset of Figs. 4A and B were plotted at another intensity scale. First, the curve obtained after crystallization from 55°C was compared with the curve obtained without thermal treatment at room temperature. The 9 nm shoulder (see arrow), which is clearly present at the descending diffraction curve of the sample without thermal treatment, disappeared after recrystallization from 55°C. In addition, the intensity of the two positions of the doublet (peaks at 1.03 and 1.41 nm^{-1}) increased. This is also the case for the intensities of the higher order diffraction peaks (see inset). Furthermore, at $Q = 0.5 \text{ nm}^{-1}$ a shoulder is still present, while the sharp peak at 1.87 nm^{-1} based on cholesterol reduced in intensity. Recrystallization from 55°C revealed only a very small change in the position of the various peaks.

As stated above, the 6 nm peak is still present at 55°C (see Fig. 4A), while both the 9.0 and 4.5 nm reflections possibly disappeared. It is likely that a part of the disordered lipids at 55°C recrystallized upon cooling in the

TABLE 1. Wide-angle X-ray diffraction (WAXD) and small-angle X-ray diffraction (SAXD) lipid spacings (nm) found as a function of temperature

Temperature	6.0 nm Phase	13.2 nm Phase	9 nm Phase ^a	Temperature	Lateral Phases	Cholesterol
25° and 50°C	6.0s, 3.0w	≈ 12w, 4.5s, ^b 3.35s, ^c 2.7m, 2.2m, 1.68m, ^c 1.54w, 1.32w	≈ 9m, 4.5s ^b	25°C	0.414s	3.35s, ^c 1.68m, ^c 0.622w, 0.573w, 0.523w, 0.484w
55°C	6.0m	≈ 12w, 3.35s, 2.7m, 2.2m, 1.68m, 1.54vw, 1.32vw	-- ^d	45°C	0.414s	3.35s, 1.68m, 0.614w, 0.565w, 0.523w, 0.497w
60°C	6.0vw	3.35m, 2.7w, 2.2w, 1.68m		60°C	0.414s ^e	3.35m, 1.68m, 0.614w, 0.565w, 0.523w, 0.497w
60° and 66°C	broad shoulder between 1 and 1.5 nm^{-1} , intensity at 66°C decreased compared to 60°C			72°C	0.414w	
72°C				95°C		

The intensities of the 12, 9, 6, 4.5, and 3 nm were based on the SAXD curve; the intensities of the other reflections were based on the WAXD pattern. The reflections at 2.7, 2.2, and 1.68 nm spacings were very weak in the SAXD curve, but clearly detectable in the WAXD pattern due to the difference sample-detector (SAXD) and sample-film (WAXD) distance (see Experimental). At 55° and 60°C, the 2.7, 2.2, 1.68, 1.54, and 1.32 nm reflections could only be detected by WAXD; s, strong; m, medium; w, weak; vw, very weak.

^aThe presence of the 9 nm phase is uncertain, see Discussion.

^bThe 4.5 nm reflection might be based on the 9.0 nm phase, and/or the 13.2 nm phase.

^cThe 3.35 and 1.68 nm reflections might be due to both crystalline cholesterol and the 13.2 nm lamellar phase.

^dThe 4.5 nm phase weakened in intensity and possibly disappeared between 50° and 55°C.

^eThe 0.414 nm reflection increased in intensity compared to 25°C.

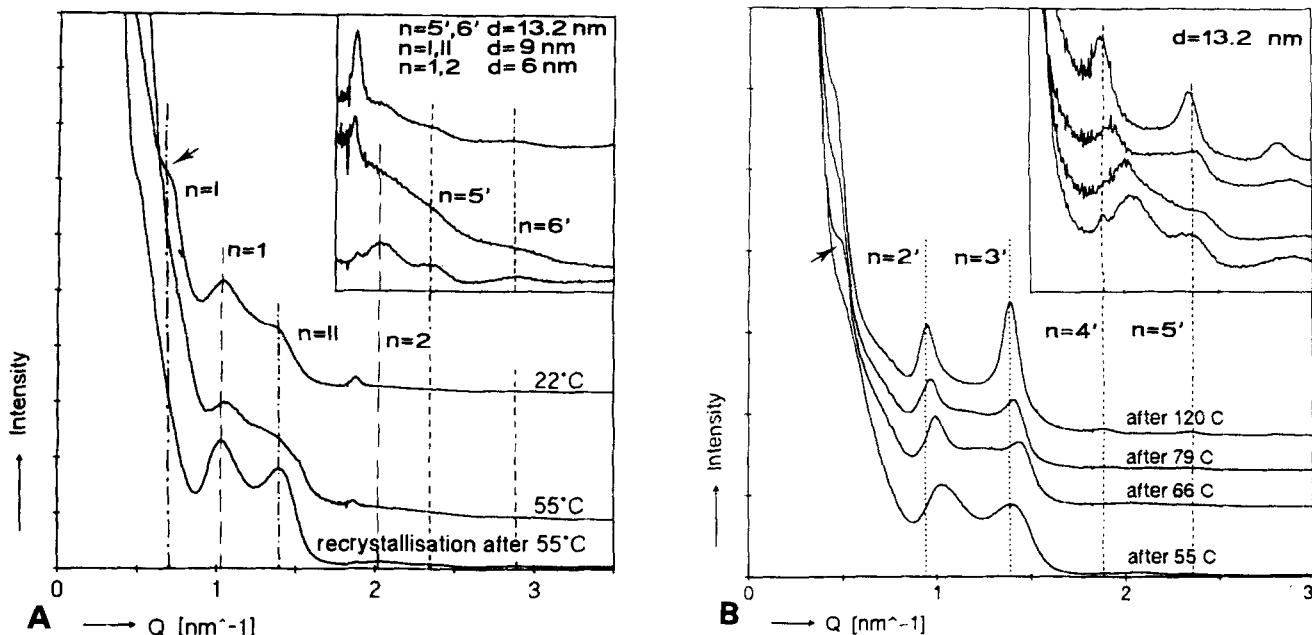


Fig. 4. A: The scattering curve after recrystallization from 55°C. The 9 nm shoulder on the descending diffraction curve disappeared (see arrow). The intensities of the various peaks located at higher Q values (see inset in the figure) increased in intensity after recrystallization at 55°C and are based on a 13.2 nm lamellar phase. The intensities are in arbitrary units. B: The scattering curves after recrystallization from various temperatures as indicated in the figure. A shift in the peak positions is noticed. The 6 and 3 nm peaks are both clearly shifted to lower Q values. Recrystallization at 120°C revealed one lamellar phase with a repeat distance of 13.2 nm. The first order diffraction peak is shown only as a shoulder on the descending diffraction curve (see arrow). The intensities are in arbitrary units; n = 2', 3', etc. denotes the orders of the 13.2 nm lamellar phase.

phase corresponding to the 6 nm reflection, as that phase could act as a template. In addition, a part of the lipids recrystallized in another phase that did not lead to a reappearance of the 9 nm shoulder, but increased the intensities of the peaks at higher Q values (smaller spacings, see inset in Fig. 4A) and resulted in a 4.45 nm peak. In the corresponding WAXD pattern also a shift from 1.54 nm (present in the control at room temperature) to a 1.45 nm spacing was observed (not shown). Recrystallization after heating to 66°C, 79°C, or 120°C resulted in patterns in which the peak positions were shifted with respect to those found in the scattering pattern of the untreated SC. As a function of increased maximum heating temperature, the peaks originally located at 6 and 3 nm were systematically shifted to higher spacings (see Table 2 and Fig. 4B) while the peaks originally located at 4.5, 2.7, and 2.2 nm spacing were shifted to lower spacings when crystallized at 66 and 79°C, but returned to their original values when recrystallized at 120°C. This confirms the statement that the 6 and 4.5 nm peaks of untreated SC are based on different phases (see above). After recrystallization at 120°C, the interpeak distances of successive peaks were equal, but the distance between the first sharp peak and the Q = 0 position was twice the interpeak distances. From this it was concluded that the first sharp peak was a second order peak and that the peaks were based on a 13.2 nm lamellar phase.

On the descending curves at 0.5 nm⁻¹ a shoulder was observed that is indicative for a weak first order peak of the 13.2 nm lamellar phase.

The cholesterol peak did not appear after crystallization at elevated temperatures. It seems that cholesterol is intercalated in the bilayers of the 13.2 nm lamellar phase.

Recrystallized lipids in stratum corneum as a function of temperature. Stratum corneum preheated to 110°C and cooled to room temperature was heated from ambient temperature to 90°C. The lamellar phase started to become disordered at approximately 55°C as indicated by the decline and

TABLE 2. Small-angle X-ray spacings of the lamellar phases after equilibration at elevated temperature followed by recrystallization

Equilibration Temperature	Spacings				
	nm				
120°C	<i>6.61^a</i>	4.48	<i>3.35</i>	2.68	2.22
79°C	<i>6.47</i>	4.44	<i>3.25</i>	2.63	2.18
66°C	<i>6.28</i>	4.35	<i>3.12</i>	2.59	2.12
55°C	<i>6.12</i>	4.45	<i>3.08</i>	2.65	2.17

The stratum corneum was heated to the desired temperature, equilibrated for 1 h, and cooled to room temperature, after which the stratum corneum was equilibrated at room temperature for 48 h at 20% hydration.

^aSpacings depicted in italics increased systematically as a function of increasing equilibration temperature.

final disappearance of the reflections. No shifts in peak positions were observed. At 72°C only a descending scattering curve was measured. There is an indication that the reflection observed at elevated temperatures on the scattering curve of the corneocyte envelope (see below) is also present (see arrow, Fig. 5).

Corneocyte envelopes

The diffraction curves of the corneocyte envelopes (i.e., corneocyte cell membrane to which lipids are chemically linked) isolated from SC were measured as a function of temperature. The corneocyte envelope was isolated from epidermis obtained either by heat separation or by dermatoming the skin. The diffraction curves measured at various temperatures are given in Fig. 6. The curve of the corneocyte envelope, isolated from epidermis obtained by heat separation, exhibits a broad peak at approximately 1.2 nm^{-1} (spacing 5.4 nm) at 25°C. This peak became sharper at higher temperatures. At 55°C and 66°C a sharp 5.35 nm peak was detected. This peak was occasionally clearly observed at scattering curves of intact SC after heating to 66 or 79°C and cooling down to ambient temperatures (not shown) and is thus not an artifact of the procedure for isolation of the corneocyte envelope from the stratum corneum. In the curves shown in Fig. 5, there is only an indication (see arrow) that this peak is present at 60°C. Apparently the peak is only observed in pre-heated corneocyte envelopes, as it was not observed in the scattering curves of corneocyte envelopes isolated from epidermis obtained by dermatoming the skin.

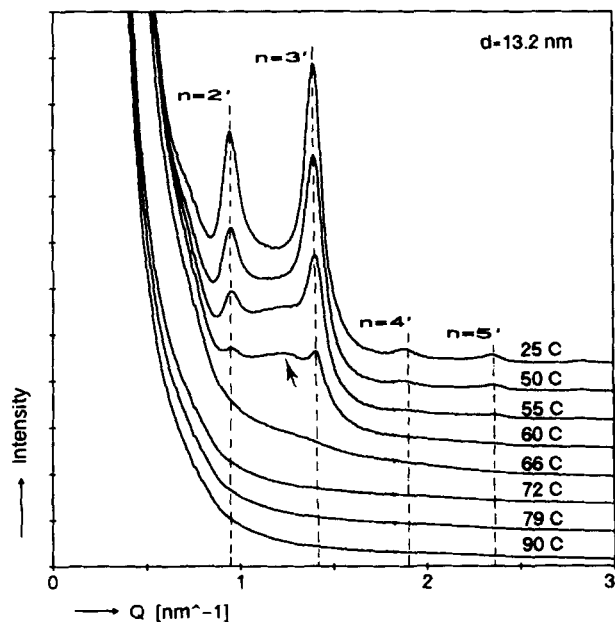


Fig. 5. The scattering curves after recrystallization at 110°C at elevated temperatures. Arrow indicates a 5.3 nm hump. The intensities are in arbitrary units; $n = 2', 3', \text{etc.}$ denotes the orders of the 13.2 nm lamellar phase.

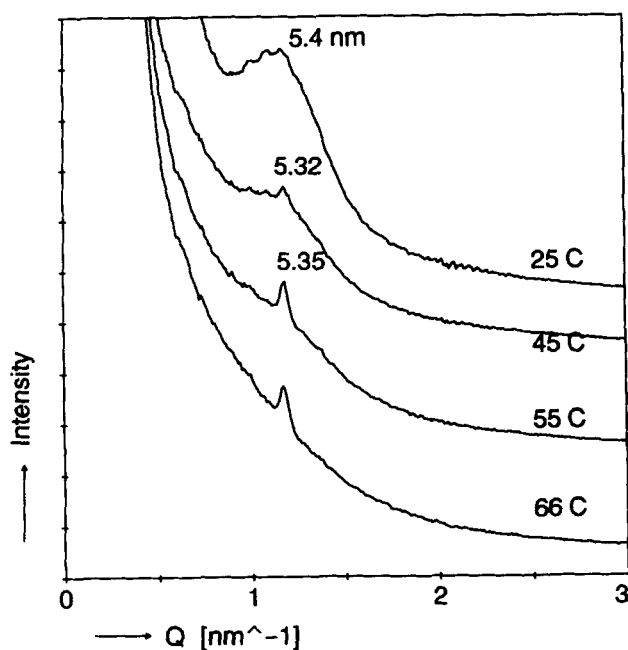


Fig. 6. The corneocyte envelope diffraction curves at various temperatures. The corneocyte envelope was hydrated to 60% w/w. The intensities are in arbitrary units.

The corneocyte envelopes were also measured as a function of temperature using WAXD. Two weak diffraction peaks were observed (not shown), at 0.414 nm and 0.463 nm. The 0.414 nm spacing is indicative for a hexagonal lateral packing of the lipids bound to the corneocyte envelopes. The 0.463 nm spacing corresponds with the β -conformation of polyglutamic acid, which is present in involucrin in the corneocyte envelope (12). This reflection was also observed in membrane couplets of mouse SC (4). The diffraction pattern did not change upon increasing the temperature to 75°C. Between 75°C and 90°C both reflections disappeared.

Chain packing

In the wide angle diffraction pattern, a large number of reflections could be detected. The spacings and reflection assignment, which are both given in Table 1, are explained below.

The diffraction pattern of pig SC oriented parallel to the primary beam is depicted in Fig. 2A. Measurements were performed at room temperature. The (arc shaped) reflections located close to the beam stop were attributed to higher order reflections of the lipid lamellar phases (see above). At higher scattering angle, a strong reflection corresponding to a 0.414 nm spacing was detected. This single spacing is characteristic for a hexagonal lateral packing of the lipids present in the SC, although the spacing is rather short. The reflection is anisotropic with highest intensity on the equator. This is indicative for a preferred orientation of the lipids perpendicular to the surface of the

tissue. The short 0.414 nm spacing corresponds to an area of 0.198 nm² per lipid molecule. The diffuse ring located at 0.46 nm might be attributed either to a liquid-crystalline phase of the lipids or to amorphous soft keratin.

After extracting the lipids with chloroform-methanol (10), the intensity of the diffuse 0.46 nm ring was considerably lowered. The reflection at 0.96 nm, characteristic for soft keratin, decreased only marginally in intensity. This indicates that lipids contribute substantially to the intensity of the 0.46-nm ring. From this we can conclude that there are at least two coexisting lipid phases in the lamellae, one with a hexagonal and the other with a liquid-like chain packing.

The diffraction patterns were also measured at various temperatures. The hexagonal reflection sharpened between 25°C and 60°C (see Fig. 2B). It appeared that the hexagonal lipid chain packing disappeared between 72 and 95°C (see Figs. 2C and 2D), but the reflection already weakened between 60°C and 72°C, which indicates that the phase change took place over a wide temperature range. Upon hydrating the SC from 6% w/w to approximately 60% w/w, no change in the position of the 0.414 nm reflection was observed. Therefore, no lateral swelling of the lipids occurs upon hydration.

Cholesterol

Several weak, but detectable, reflections were observed at 0.484, 0.523, 0.571, and 0.622 nm spacings. The reflections were anisotropic with lower intensity on the meridian. This pattern was attributed to anhydrous crystalline cholesterol (16). The non-isotropic character is indicative for a preferred orientation of cholesterol in the SC. Furthermore, two additional arcs located on the meridian at 3.35 and 1.68 nm spacings were at least partly attributed to crystalline cholesterol. The preferred orientation of the reflections strongly suggested that the longest axis of the cholesterol lattice (3.35 nm) is orientated perpendicular to the SC surface. This is parallel to the dominant orientation of the lipids. It is likely that cholesterol crystals were intercalated in the bilayers of the intercellular lamellar phases in such a way that the longest axis of the cholesterol crystals points in the same direction as the stacking direction of the lamellar sheets.

Upon increasing the temperature to 45°C, the diffraction pattern of cholesterol changed. At 45°C the reflections were located at 0.497, 0.515, 0.523, 0.565, and 0.614 nm. The change in pattern is due to a polymorphic transition of anhydrous cholesterol at approximately 40°C, that was also found in the pure substance (17). The cholesterol reflections disappeared between 60 and 72°C, which indicates a higher solubility of cholesterol in the lipid mixture, probably due to the liquid state at higher temperatures. After incubation of SC at high temperatures and recrystallization, the cholesterol reflections did not reappear in the

diffraction patterns. Probably cholesterol becomes incorporated into lipid lamellar phases during heating and recrystallization.

Keratin

The diffraction pattern exhibits two diffuse rings, located at approximately 0.46 and 0.96 nm (see Fig. 2A). On the diffuse ring at 0.96 nm two diffuse spots are located on the meridian. These are assigned to poorly developed α -keratin, although the diffuse arc characteristic for α -keratin (expected at 0.515 nm spacing on the equator) cannot be detected with certainty as it is partially obscured by the very broad diffuse ring at 0.46 nm spacing. In the same samples, two reflections were located on the equator at 0.510 and 0.532 nm. These reflections resulted from pig hair, which was not always completely removed from the stratum corneum samples. The presence of these reflections made it even more difficult to detect the 0.515 nm diffuse reflection of poorly developed keratin. The α -keratin reflections did not change upon increasing the temperature to 120°C. No α to β conformational change was observed.

Perpendicular orientation of stratum corneum sheets

In perpendicular orientation of the sheets to the primary beam, the diffraction pattern of pig SC does not exhibit the various arcs close to the beam stop, which again is an indication of a dominant orientation of the lamellae parallel to the SC surface. Furthermore, the α -keratin spots at 0.97 nm spacing were not present, which indicated a preferred orientation of α -keratin parallel to the surface of the stratum corneum. The cholesterol reflections at 0.622, 0.571, 0.523, and 0.484 nm appeared to be isotropic. In addition, the 1.68 nm and 3.35 nm arcs could not be detected. Both observations confirm the suggestion that the cholesterol crystals are orientated with the longest lattice axis perpendicular to the surface of the SC, i.e., in the same direction as the lamellar stacking.

DISCUSSION

First, the interpretation of the diffraction peaks based on the lamellar phases will be discussed, then the lipid structure of pig SC will be compared with that found in human and mouse SC.

Interpretation of the reflections based on the lamellar phases

The diffraction curve and the diffraction pattern obtained by SAXD and WAXD are very complicated, but can be interpreted as follows.

As indicated in the various figures, the 6.0 nm ($Q = 1.05 \text{ nm}^{-1}$) and 3.0 nm ($Q = 2.09 \text{ nm}^{-1}$) diffraction peaks originate from one lamellar phase: recrystallization

from 66°C and 72°C resulted in a shift of both peaks to lower Q values, while all other peaks slightly shifted to higher Q values. If the peak at 1.05 nm^{-1} is of first order, the repeat distance of the lamellar phase is 6 nm and the 2.10 nm^{-1} peak is of second order. Because a shoulder is located at the descending diffraction curve corresponding to a spacing of 12 nm, there is the possibility that the peak at 1.05^{-1} nm is actually the second order. However, in this case the 3rd, 5th, and 6th order diffraction peaks could not be detected, which makes it unlikely for a 12 nm lamellar phase to be present. It seems that the 6 nm lamellar phase is the most reasonable explanation. Recently, the phase behavior of isolated pig ceramides and cholesterol has been studied. The results of these studies confirm the presence of a 6 nm lamellar phase (J. A. Bouwstra, K. Cheng, A. Weerheim, G. S. Gooris, and M. Ponc, unpublished results).

The diffraction peaks (SAXD curve) and arcs (WAXD pattern) corresponding to 2.67 nm ($n = 5$), 2.17 nm ($n = 6$), 1.32 nm ($n = 10$) spacings and possibly also 3.35 nm ($n = 4$) and 1.67 nm spacings ($n = 8$), both obscured by crystalline cholesterol (see above), can be attributed to a lamellar phase with a repeat distance of 13.2 nm (see Figs. 4A and B). A 13.2 nm lamellar phase was also found after lipid crystallization from 120°C (Fig. 5). It is even possible that the reflection at 4.5 nm ($n = 3$) originates partly from the 13.2 nm lamellar phase (not indicated in the figures). The first order peak of this lamellar phase is very weak, which was also observed in human SC and it is therefore not unlikely that the shoulder at approximately 12 nm spacing found on the descending scattering curve is, in fact, the distorted first order diffraction peak of a 13.2 nm lamellar phase. The discrepancy between the calculated and expected positions of the first order diffraction peak can be caused by the location of the peak on the steeply descending diffraction curve. This makes localization of the peak position difficult. Furthermore, in this part of the curve, a small change in peak position results in a large change in spacing. In addition, in poorly repeating lattices such as the lipid structures of pig SC, the position of the diffraction peak is influenced by the electron density distribution in the lattice (form factor). This is especially noticeable for peak positions close to the primary beam position ($Q = 0 \text{ nm}^{-1}$).

There are two reflections that could not be attributed to either 6 or 13.4 nm lamellar phases. These are the 9 nm shoulder ($Q = 0.7 \text{ nm}^{-1}$) on the steep descending scattering curve and the 1.52 nm reflection (WAXD pattern). Both reflections disappeared after recrystallization from 55°C (see Fig. 4A) and might be attributed to a third lamellar phase. The 9 nm shoulder should then be of 1st order and the 1.52 nm reflection of 6th order. It is also possible that the 4.5 nm reflection is partly due to the 9 nm lamellar phase, as the 4.5 nm and 9 nm reflections both decreased in intensity and possibly disappeared at

55°C (see Fig. 3). It is difficult to get more evidence for the presence of the 9 nm lamellar phase from diffraction experiments, as the higher order reflections (3 ($n = 3$), 2.25 ($n = 4$), and 1.8 nm ($n = 5$)) were all obscured by the higher order reflections of the two other lamellar phases.

The presence of more than one lipid phase was confirmed by two recent studies. First, in mixtures of cholesterol and pig ceramides in various ratios (J. A. Bouwstra, K. Cheng, A. Weerheim, G. S. Gooris, and M. Ponc, unpublished results) the 6.0 and 13.2 nm phases were found. Second, two lipid phases with repeat distances of 10.4 and 5.3 nm were reported (13) to be present in brain ceramides and cholesterol mixtures. Electron microscopic visualization of stratum corneum with RuO_4 post-fixation revealed the presence of a sequence of broad-narrow-broad electron-translucent bands between which electron-dense bands were located (10, 12). When calculating the broad-narrow-broad periodicity from these micrographs, the periodicity appeared to be approximately 13 nm, which is in excellent agreement with the longest periodicity found in this study. However, the 6.0 nm periodicity was never observed by electron microscopy. This is still very puzzling and until now no adequate answer is given for this inconsistency between X-ray diffraction and electron microscopic results. One could speculate that in using the RuO_4 post-fixation technique, small differences in lipid organization might be masked, because one visualizes the location of the ruthenium and not the lipid structure itself. Besides this inconsistency, excellent agreement was found between results obtained with the two techniques, especially concerning the electron-density distribution within the 13.4 nm periodicity. Most of these electron-density calculations were carried out using the diffraction patterns of human (6) and mouse skin (8). The calculations were performed using the X-ray diffraction curves obtained after recrystallization of the lipids in the stratum corneum from 120°C, as only then an adequate resolution of the peaks based on the 13-nm periodicity was obtained. The calculations revealed a broad-narrow-broad sequence of electron-lucent regions perpendicular to the basal plane that most likely correspond with the hydrocarbon regions. Between these electron-lucent regions, electron-dense regions were located that were very large, being 1.45 and 2.9 nm in width. As we mainly deal with ceramides, free fatty acids, and cholesterol, the head-group regions were not expected to exceed 1.0 nm in width. To explain the large head-group regions, incorporation of proteins in the lipid structure was suggested (6). The same inconsistency between the type of lipids present and the large head-group regions arose when electron density calculations were carried out with pig stratum corneum (not published); the intensities of the various peaks could not be fitted with narrow electron-dense regions, not exceeding 1.0 nm in width.

Electron microscopy using RuO₄ post-fixation revealed a broad-narrow-broad sequence of the electron-lucent bands in the intercellular lamellar pattern of mouse, pig, and human stratum corneum, as already described above. In comparing the results obtained by electron microscopy and X-ray diffraction, one can conclude that an excellent agreement exists with regard to the broad-narrow-broad sequence of the electron-lucent bands. If one further assumes that, after fixation, ruthenium is associated with the head-groups, the electron-lucent bands resulting from both techniques correspond with the hydrocarbon regions. In fact, the models proposed by Wertz and Downing (3) and by Downing (12) are based on the assumption that ruthenium is associated with the head-group regions.

Despite the agreement between the results obtained by both techniques, many questions concerning the phase behavior of skin lipids still remain. In the future we hope to answer some of the questions by studying the phase behavior of lipid mixtures isolated from stratum corneum.

Comparison of lipid and protein structures of different species

In human SC, two lamellar phases with repeat distances of 6.4 and 13.4 nm were detected. In mouse SC, in most cases only the 13.4 nm lamellar structure was present. Only occasionally, a 6 nm lamellar phase was observed. Whether these differences in lamellar structure account for the differences in diffusion rate through stratum corneum is not yet clear, but the best defined lipid structure is located in mouse SC, which is also the most permeable tissue compared to pig and human SC. If indeed differences in lamellar stacking are responsible for differences in diffusional resistance of the skin, the results indicate that the 13 nm structures should be more permeable to drugs than the 6 nm lamellar phase. Furthermore, the number of phase boundaries of the two lamellar phases is expected to be less in mouse stratum corneum compared to human and pig stratum corneum, since the 6 nm phase is only occasionally observed.

The similarity in structure after recrystallization of the lipid from 120°C is remarkable. Independent of the species, only the 13 nm lamellar structure was found. With respect to the lateral packing of the lipids also, differences in structure exist. In human and mouse SC an orthorhombic and possibly a hexagonal lipid packing were present (7). The presence of a liquid-like packing was not obvious in human SC. In mouse SC a substantial amount of the lipids form a liquid crystalline phase (4, 8). As mentioned before, mouse SC is more permeable than human SC (18). It is very likely that, besides differences in tortuosity of the transport route and differences in thickness of the stratum corneum, the amount of lipids in a liquid-like phase plays a dominant role in the differences in transport rate in the various species. Not only is the


diffusional resistance of a liquid phase lower than that of a crystalline phase (19), but an increase in liquid-like chain packing also increases the number of phase boundaries of the coexisting phases. As already suggested by others (16, 20), an increase in the number of phase boundaries might be responsible for an increase in the permeability of the SC. It has been shown in phospholipid systems that creation of phase boundaries lowers the diffusional resistance dramatically (20).

In our diffraction studies of pig SC, no evidence has been found for the presence of an orthorhombic structure. Fourier transform infrared spectroscopy studies revealed an orthorhombic structure in pig SC based on the splitting of the CH₂ scissoring mode of the 1470 cm⁻¹ band of pig SC (21). The discrepancy between these studies is not yet understood.

Crystalline cholesterol was observed in all three species, but in mouse stratum corneum it was detected only occasionally. In human SC it was detected frequently, while in pig SC it was always detected (SC of five pigs was measured). In all three species the cholesterol reflections disappeared after heating to 120°C and recrystallization to ambient temperature.

With respect to keratin, clear differences also exist between the various species. In mouse SC only a very weak 0.96 nm diffuse ring was observed, while in human SC the 0.96-nm diffuse ring is strong in intensity. This indicates that human SC contains more amorphous keratin than mouse SC. In parallel orientation of the SC sheets with respect to the primary beam, the diffuse 0.96 nm ring in human SC is slightly anisotropic. In pig SC, the anisotropy was more pronounced; two spots on the meridian could be detected (see Fig. 2). The most likely explanation is the presence of α -keratin in pig SC, while this is almost absent in human SC.

Cholesterol

Crystalline cholesterol reflections were observed in both the wide- and small-angle X-ray patterns. In model systems of pig ceramides and cholesterol prepared in buffer solution, cholesterol monohydrate starts to phase-separate at a ceramide/cholesterol molar ratio of 0.6 (17). In these lipid mixtures only cholesterol monohydrate was found. It is possible that cholesterol monohydrate is also present in intact SC, but that due to the storage of SC over silica gel, cholesterol monohydrate transformed to cholesterol anhydride. The hydration of SC over water for 24 or 48 h seems to be insufficient to hydrate cholesterol crystals. 

We thank the Netherlands Organization for Scientific Research (NWO) for financial support and for the provision of experimental time at the SRS.

Manuscript received 13 June 1994 and in revised form 10 November 1994.

REFERENCES

- Boddé, H. E., M. A. M. Kruithof, J. Brussee, and H. K. Koerten. 1989. Visualization of normal and enhanced H₉A₂ transport through human skin in vitro. *Int. J. Pharm.* **53**: 13-24.
- Schurer, N. J., and P. M. Elias. 1992. The biochemistry and function of stratum corneum lipids. *Adv. Lipid Res.* **24**: 27-56.
- Wertz, P. W., and D. T. Downing. 1991. Physiology, Biochemistry and Molecular Biology of the Skin. 2nd Edition. L. A. Goldsmith, editor. Oxford University Press, Oxford. 205-236.
- White, S. H., D. Mirejovsky, and G. I. King. 1988. Structure of lamellar lipid domains and corneocyte envelopes of murine stratum corneum: an X-ray diffraction study. *Biochemistry.* **27**: 3725-3732.
- Garson, J.-C., J. Doucet, J.-L. Leveque, and G. Tsoucaris. 1991. Oriented structure in human stratum corneum revealed by X-ray diffraction. *J. Invest. Dermatol.* **96**: 43-49.
- Bouwstra, J. A., G. S. Gooris, J. A. van der Spek, and W. Bras. 1991. Structural investigations of human stratum corneum as determined by small angle X-ray diffraction. *J. Invest. Dermatol.* **97**: 1004-1012.
- Bouwstra, J. A., G. S. Gooris, M. A. Salomons-de Vries, J. A. van der Spek, and W. Bras. 1992. The structure of human stratum corneum: a wide angle X-ray diffraction study. *Int. J. Pharm.* **84**: 205-216.
- Bouwstra, J. A., G. S. Gooris, and W. Bras. 1994. The lipid and protein structure of mouse stratum corneum. *Biochim. Biophys. Acta.* **1212**: 183-192.
- Hou, S. Y., A. K. Mitra, S. H. White, G. K. Menon, R. Ghadially, and P. Elias. 1991. Membrane structures in normal and essential fatty acid-deficient stratum corneum: characterization by ruthenium tetroxide staining and X-ray diffraction. *J. Invest. Dermatol.* **96**: 215-223.
- Swartzendruber, D. C. 1992. Studies of epidermal lipids using electron microscopy. *Semin. Dermatol.* **11**: 157-161.
- Fartasch, M., I. D. Bussakas, and T. L. Diepgen. 1992. Disturbed extruding mechanism of lamellar bodies in dry non-eczematous skin of atopics. *Br. J. Dermatol.* **127**: 221-227.
- Downing, D. T. 1992. Lipid and protein structures in the permeability barrier of mammalian epidermis. *J. Lipid Res.* **33**: 301-314.
- Parrot, D. T., and J. T. Turner. 1993. Mesophase formation by ceramides and cholesterol, a model for stratum corneum lipid packing? *Biochim. Biophys. Acta.* **1147**: 273-276.
- Swartzendruber, D. C., D. J. Kitko, P. W. Wertz, K. C. Madison, and D. T. Downing. 1988. Isolation of corneocyte envelopes from porcine epidermis. *Arch. Dermatol. Res.* **280**: 424-429.
- Van Hal, D., E. Jeremiase, H. E. Junginger, F. Spies, and J. A. Bouwstra. 1994. Structure of hydrated human stratum corneum and influence of application of non-ionic surfactant vesicles: a freeze fracture electron microscopic study. *Proceedings of the International Symposium on Controlled Release of Bioactive Material.* **21**: 168-169.
- Bogren, H., and K. Larsson. 1963. An X-ray diffraction study of crystalline cholesterol in some pathological deposits in man. *Biochim. Biophys. Acta.* **75**: 65-69.
- Loomis, C. R., G. G. Shipley, and D. Small. 1979. The phase behavior of hydrated cholesterol. *J. Lipid Res.* **20**: 525-535.
- Potts, R. O., and R. Guy. 1993. The prediction of percutaneous penetration, in dermal and transdermal drug delivery, R. Gurny and A. Teubner, editors. Wissenschaftliche Verlagsgesellschaft mbH, Stuttgart. 153-160.
- Small, D. 1986. The Physical Chemistry of Lipids: From Alkanes to Phospholipids. Plenum Press, New York. 523.
- Ongpipattanakul, B., R. R. Burnette, R. O. Potts, and M. L. Francoeur. 1992. Solid phase behavior of lipids in porcine stratum corneum. *Proceedings of the International Symposium on Controlled Release of Bioactive Material.* **19**: 143-144.
- Wu, S. H. W., and H. M. McConnell. 1973. Lateral phase separation and perpendicular transport in membranes. *Biochem. Biophys. Res. Commun.* **55**: 484-491.